JOURNAL OF MATERIALS SCIENCE 29 (1994) 786–799

Compressional behaviour of carbon fibres

Part II *Modulus softening*

N. MELANITIS, P. L. TETLOW, C. GALIOTIS*
Materials Department, Queen Mary and Westfield College, Mile End, London E1 4NS, UK
S. B. SMITH
Courtaulds Research, P.O. Box 111, 101 Lockhurst Lane, Coventry CV6 5RS, UK

Spectroscopic–mechanical studies have been conducted on a range of carbon fibres by bonding single filaments on the top surface of a cantilever beam. Such a loading configuration allows the acquisition of the Raman spectrum of carbon fibres and the derivation of the Raman frequency strain dependence in tension and compression. Strain hardening phenomena in tension and strain softening phenomena in compression were closely observed. The differences in the slopes of the Raman frequency versus applied strain curves in tension and compression respectively, have been used to obtain good estimates of the compression moduli. A method of converting the fibre Raman frequency versus strain data into stress–strain curves in both tension and compression, is demonstrated. Values of fibre stress and fibre modulus at failure in compression compare exceptionally well with corresponding estimates deduced from full composite data. The mode of failure in compression has been found to depend upon the carbon fibre structure. It is demonstrated that certain modifications in the manufacturing technology of PAN-based fibres can lead to fibres which show resistance to catastrophic compressive failure without significant losses in the fibre compressive modulus.

1. Introduction

1.1. Compressional behaviour of composites: the role of fibres

The study of the compressional behaviour of carbon fibre composites has attracted a significant volume of research, mainly as a result of the increasing exploitation of these materials in aerospace and marine applications. For design purposes, parameters such as the Young's modulus, strength and mode of failure in compression, have to be well specified. This has led over the years to the development of a number of compression tests which employ simple coupon geometries subjected to axial compression [1–5]. It is worth noting that the type of test selected usually affects the property it sets out to measure, because the loading configuration in each case introduces a specific stress field [4]. In particular, the problem of shear concentration at or near the grips has been addressed and alternative compression tests have been developed [6].

Non-linear phenomena have been observed during mechanical loading of carbon fibre composites in tension [7–9]. These strain-hardening effects were attributed to the stress–strain behaviour of the reinforcing fibres themselves [10, 11]. More recently, experimental evidence has been provided for modulus softening during compression loading of carbon fibre composites [4, 5]. A reduction of composite modulus up to 30% of its initial value, at a compressive strain of 1% has been recorded [4].

It has been widely assumed that fibre waviness and/or misalignment play a significant role in (a) determining the failure stress of the unidirectional composites and in (b) modulus reduction with applied strain in compression. An alternative explanation that would apply to carbon fibre composites is that the fibres themselves show a non-linear response in compression and effectively soften at higher strains [3, 12, 13]. If misalignment were the main cause of non-linearity, one would assume that the stress–strain characteristics of most continuous fibre composites would be non-linear. However, the stress–strain curves of glass fibre composites in tension and compression, are fairly linear up to high values of applied strain and this reflects well the behaviour of the fibre themselves [3, 13]. It seems, therefore, that the non-linear effects in composites are only associated with reinforcing fibres such as carbon [12] or aramid [14], which exhibit non-linear responses to an applied load. Additional evidence for the influence of the fibre modulus softening upon the stress–strain characteristics of carbon fibre composites will be provided here.

1.2. Compressional behaviour of single fibres

Various methods have been employed for the determination of the compressive properties of single filaments such as the elastic loop test [15, 16], the single fibre model composite test [17, 18], the cantilever

* Author to whom all correspondence should be addressed.

0022–2461

beam test [19, 20], the four-point bending test [21] and the single-fibre recoil test [22]. The application of these tests is normally limited to the detection of failure mode and the estimation of the compressive strength by assuming that the compression Young's modulus is equal to the Young's modulus in tension. In the first paper of this series [12], a modified version of the cantilever beam was employed to compress the fibre axially and the applied strain in the fibre was monitored with laser Raman spectroscopy (LRS). This technique involved the application of small and defined compressive strains to single filaments by bonding them to one side of a cantilever beam which was subsequently bent to subject the fibres to a gradient of compressive load. The strain build up along the fibre was monitored point-by-point with a laser Raman microprobe and optical microscopy. This enabled (a) the determination of the critical strain for compression failure and the mode of failure for fibres of different modulus, (b) an assessment of the fibre strain take-up in the post-failure region and, finally, (c) the derivation of the compression modulus by assuming a linear dependence between Raman frequency and applied strain. Experiments performed on a range of PAN-based carbon fibres of tensile moduli ranging from 230–400 GPa, showed that high modulus fibres fail by shear while low and intermediate modulus fibres exhibit a "bulging" mode of failure [12]. The Young's modulus of all fibres examined was found to soften considerably in compression.

In this work, the behaviour of a number of carbon fibres in both tension and compression was studied in detail in an attempt to determine the dependence of the compression modulus upon applied compressive strain and hence provide estimates of the critical compressive stress to fibre failure. The physical requirement for a smooth transition through the zero strain point of the Raman frequency versus tension and compression strain data, is obeyed. Henceforth, a method for deriving stress-strain plots in both tension and compression for single carbon fibre filaments, will be demonstrated.

2. Background

2.1. Study of carbon-fibre structure using laser Raman spectroscopy

Carbon fibres owe their exceptional thermomechanical properties to the nature of the basic graphitic structural unit [23, 24]. A large number of investigations have been carried out in an attempt to detect and model the structural features of carbon fibres. In general, carbon fibres are thought to consist of blocks of graphite layer planes, denoted as crystallites [25, 26]. These crystallites are crumpled along the fibre axis like sheets of paper, thus allowing irregular pores and defects to develop in their boundaries [27]. The parameters required for a complete characterization of the fibre structure comprise primarily the crystallite length, L_a, the crystallite thickness, L_c, the curvature of the crystallite layers, r_1, and the distribution of angle orientation of the crystallite units $l(\phi)$ [26].

Laser Raman spectroscopy has been successfully employed in recent years for the surface characterization of carbon fibres [28–31]. The Raman spectrum of carbon fibres comprises a number of frequency bands, each one assigned to a certain structural configuration. Only one Raman line has been indisputably identified. This is the so-called G-line [32], located at 1580 cm^{-1} (Fig. 1), and assigned to the E_{2g} vibrational mode of the graphite crystal [28]. The appearance of other bands in the Raman spectrum of carbon fibres indicates the presence of some form of "disordered" structure on the carbon-fibre surface. The most prominent "disorder"-induced feature in the carbon-fibre Raman spectrum is the so-called D-line [32], appearing at about 1360 cm^{-1} (Fig. 1). This has been attributed to the increase in the amount of crystallite boundaries with decreasing crystal size [29], or to the presence of graphite edge planes perturbing the smoothly stratified crystallites of the fibre surface, or both [30].

The increase in the heat-treatment temperature (firing temperature), yields a fibre product with highly oriented, larger crystallite units, resulting in a higher fibre Young's modulus [23, 24]. The Raman spectrum of such a fibre exhibits a pronounced, narrow and intense G-line and decaying "disorder"-induced features. A measure of the fibre surface crystallinity is given by the intensity ratio I_D/I_G of the D and the G-lines of the carbon fibre Raman spectrum. It has been found that this ratio is inversely proportional to the crystallite size, L_a [29]. More recent work, however, has also provided evidence for the dependence of this ratio upon the orientation of the basic crystallite unit regardless of the size of L_a [30]. Additional evidence will be presented in a future publication [33].

Application of tensile load on single carbon fibres has shown that all Raman frequencies of carbon fibres are sensitive to applied strain [33–36]. The negative shift of the Raman frequency with applied strain has been attributed to the anharmonicity of the interatomic force constant of the graphitic bond [37, 38]. The rate of Raman frequency shifting with strain is defined as the Raman frequency gauge factor (RFGF)

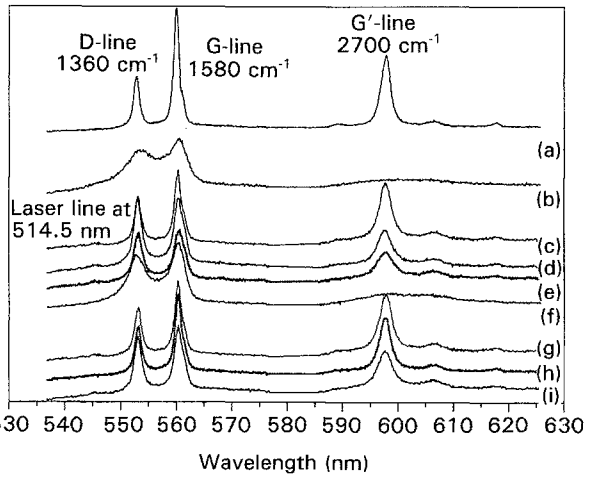

Figure 1 The Raman spectrum of nine carbon fibre types as a function of wavelength. The laser excitation wavelength was 514.5 nm: (a) A1, (b) A2, (c) B1, (d) B2, (e) B3, (f) B4, (g) C1, (h) C2 and (i) C3.

for the particular vibrational mode and at a first approximation, had been considered to be constant [39].

With respect to the graphitic G-line, the higher the fibre surface crystallinity, the greater is the (absolute) value of the RFGF. This is due to the fact that, in highly crystalline fibres, the externally applied axial stress is almost fully delivered to individual graphite bonds. For fibres with a lower degree of crystallinity, a significant amount of the external deformation is consumed into bending, folding and rotational deformations at the expense of bond-stretching deformations [33]. A full account of the characterization of carbon fibres using laser Raman spectroscopy, the effect of tensile load on the Raman frequencies and the information about the fibre structure derived from the above investigations, will be presented elsewhere [33].

3. Experimental procedure

3.1. Materials

The carbon fibres of this project were supplied by Courtaulds Grafil plc and had been subjected to a commercial surface treatment. The fibres are classified into three general categories with respect to their diameter and their manufacturing technology. Details of their diameter and processing parameters are listed in Table I and their mechanical properties are shown in Table II.

Group A consists of two 7 μm diameter fibres produced by a "first generation" manufacturing technology. Acrylic filaments were wet-spun and drawn in hot water and saturated steam to a total draw ratio of 14 times (Table I), to yield a final diameter of approximately 12 μm. The filaments were stabilized in hot air until the density had risen to 1.38–1.40 g cm^{-1}, using a rising-ramped temperature regime (225–245 °C). Primary carbonization was carried out using a maximum temperature of 950 °C, whilst secondary carbonization and graphitization utilized ultimate firing temperatures (UFT), up to 2600 °C, depending on modulus (Tables I and II). No additional drawing processes were carried out. During the stabilization, the filaments were held at constant length, whilst during the carbonization and graphitization, a 5% shrinkage was allowed (Table I). The A1 and A2 fibres are identical to the commercial Courtaulds Grafil HMS and XAS fibres, respectively [12].

Group B consists of four "high performance" 5 μm diameter fibres, produced using principles described elsewhere [40, 41]. Acrylic filaments were wet-spun and drawn as described above (Group A). The filaments were then subjected to a multi-stage pre-stabilization drawing at temperatures up to 270 °C (Table I), followed by stabilization as described above. Carbonization and graphitization were carried out with the filaments held at constant length (Table I). The UFT values for these fibres are also given in Table I. It is worth mentioning here that the B4 fibre is identical to the Courtauld Grafil IM-43750 fibre examined in the first paper of this series [12].

Group C consists of three approximately 6 μm diameter fibres of similar Young's modulus but of distinctly different morphologies. These fibres were prepared so as to illustrate the influence of lateral crystal size development, L_c, and axial orientation, on the compressive strength of fibres and composites. The lateral growth of graphitic crystals is primarily responsive to UFT, whilst orientation is determined by a combination of drawing steps and UFT (Table I). Accordingly, these fibres were produced by varying

TABLE II Materials properties

Fibre	Group	Diameter /μm	Young's modulus /GPa	Tensile strain to failure/%
1	A	7	390	0.9
2		7	230	1.6
1	B	5	405	1.1
2		5	375	1.3
3		5	335	1.5
4		5	305	1.8
1	C	6	378	0.9
2		6	378	1.1
3		6	364	1.1

TABLE I Materials properties

Fibre	Group	Diameter/μm	Pre-stabilization drawing (up to 245 °C)	Stabilization drawing (up to 270 °C)	Carbonization drawing (up to 950 °C)	Ultimate graphitization temperature °C
1	A	7	14	Constant length	5% shrinkage	2600
2						1350
1	B	5	14	Multi-stage	Constant length	2300
2						2200
3						1900
4						1750
1	C	6	14	1.30	10% shrinkage	2600
2				1.20	Constant length	2400
3				1.10	1.1	2200

TABLE III Structural parameters of Group C fibres[a]

Fibre	Tensile strength (GPa)	Azimuthial full width at half height (°C[b])	Crystallite size L_c^c (nm)
1	4.0	20°	6.0
2	4.1	21°	4.4
3	4.2	22°	3.4

[a] Carbon fibre modulus was maintained at constant value of about 375 GPa.
[b] The azimuthial full-width at half-height, $F002$, is measured from the X-ray diffraction of the 002 plane.
[c] The L_c was calculated using Scherrer's equation, assuming that all peak broadening is attributed to crystallite size effects.

draw regimes and UFT to achieve a similar final modulus value of approximately 370 ± 10 GPa. The structural parameters of these fibres are shown in Table III.

3.2. Specimen preparation – laser Raman spectroscopy

The specimens were prepared by aligning single carbon fibres parallel to the length of PMMA bars and approximately at the centre of their width. The thickness of the bar was 5.5 ± 0.1 mm and the width 10.0 ± 0.1 mm, respectively. The fibres were bonded to the bar using a thin clear acrylic spray (Krylon), the thickness of which did not exceed 10 μm. The film was allowed to set in a vacuum oven and at room temperature for several hours. The specimens were subsequently positioned on the cantilever beam assembly and were deflected to the required direction. Further details of the specimen preparation procedure are given in the first paper of the series [12].

In order to study the validity of the beam-theory calculations [42] and to assess the effect of creep upon our method of strain measurement, a 6 mm thick PMMA bar was loaded incrementally to a maximum 3.0% strain (9.3 mm deflection). The strain each time was measured with a strain gauge attached to the beam outer surface. In Fig. 2, the strain measured with the strain gauge is plotted against the strain calculated by means of the beam theory [42]. As can be seen, an excellent agreement is obtained up to 1.3%–1.5% and a maximum deviation of the order of 7% is observed at 3% strain. In this work, the maximum deflection was always kept below 1.3%–1.5% strain so a strain correction was not needed. In a future publication [43], the compressional behaviour of fibres such as the A2 will be assessed under extreme values of applied compressive strain.

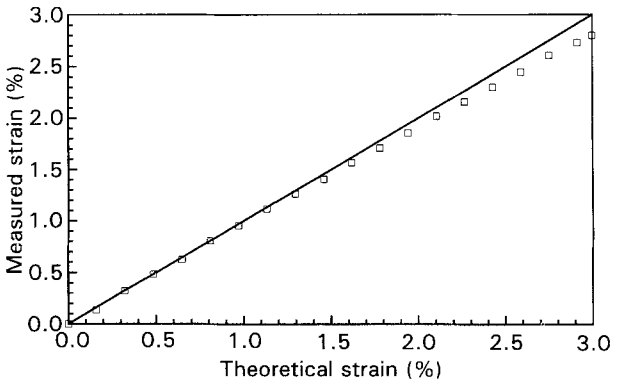

Figure 2 The measured compressive strain as a function of calculated compressive strain [40] for a 6 mm thick PMMA cantilever bar loaded to 3% strain.

Raman spectra were obtained using the 514.5 nm excitation wavelength of an argon-ion Lexel laser. The laser beam was directed through a set of mirrors and filters to a modified Nikon microscope and then focused to a 2 μm diameter spot on the fibre by means of a X50 microscope objective. The power of the incident laser beam was always retained at 1 mW to avoid over heating of the carbon fibres. The backscattered beam was collected by the same microscope objective and focused via a spatial filter assembly on the entrance slit of a triplemate SPEX 1877 spectrometer. The analysed light was subsequently dispersed on the chip of a Wright Instruments Charge Coupled Device (CCD) camera, employed as the photon detector. The camera was interfaced with a PC computer and data acquisition as well as data analysis, were controlled by dedicated software. Lorentzian distribution routines were fitted to the raw spectroscopic data. The position (Raman frequency) and the width of the Raman bands were calculated with an accuracy of ± 0.5 cm^{-1}.

4. Results

4.1. Characterization of carbon fibres using LRS

The Raman spectra of the ten fibre types studied in this work are shown in Fig. 1 over the 700–3500 cm^{-1} frequency range. As can be seen, three prominent peaks at 1360 cm^{-1} (D-line), 1580 cm^{-1} (G-line) and 2700 cm^{-1} (G-line), are obtained for most fibres employed in this work.

In Fig. 3a–c, the actual Raman scattering intensity over a narrower frequency window is presented for the G-line of all fibres of Groups A, B and C, respectively. As is apparent for most fibres, the E_{2g} peak at 1580 cm^{-1} (G-line) can be clearly resolved from the Raman feature at 1620 cm^{-1} (D'-line) which is also associated with the presence of disorder on the carbon fibre surface [29, 30]. However, for low-modulus/low-crystallinity fibres such as the A2 and IM43, the two peaks cannot be resolved and therefore the unresolved doublet at approximately 1600 cm^{-1}, will be taken as the "G-line" in this case.

The exact position of the graphitic G-line for each fibre type and its respective full-width at half-maxima (FWHM), are listed in Table IV. In addition, the ratio l_D/l_G, of the intensities of D to G lines for each fibre, are also listed in Table IV. The following general observations can be made here:

(a) within the same fibre series, the higher the fibre modulus (Table II), the lower is the intensity ratio l_D/l_G (Table IV);

(b) the higher the fibre crystallinity (Group C, Table III), the lower is the intensity ratio l_D/l_G (Table IV); and

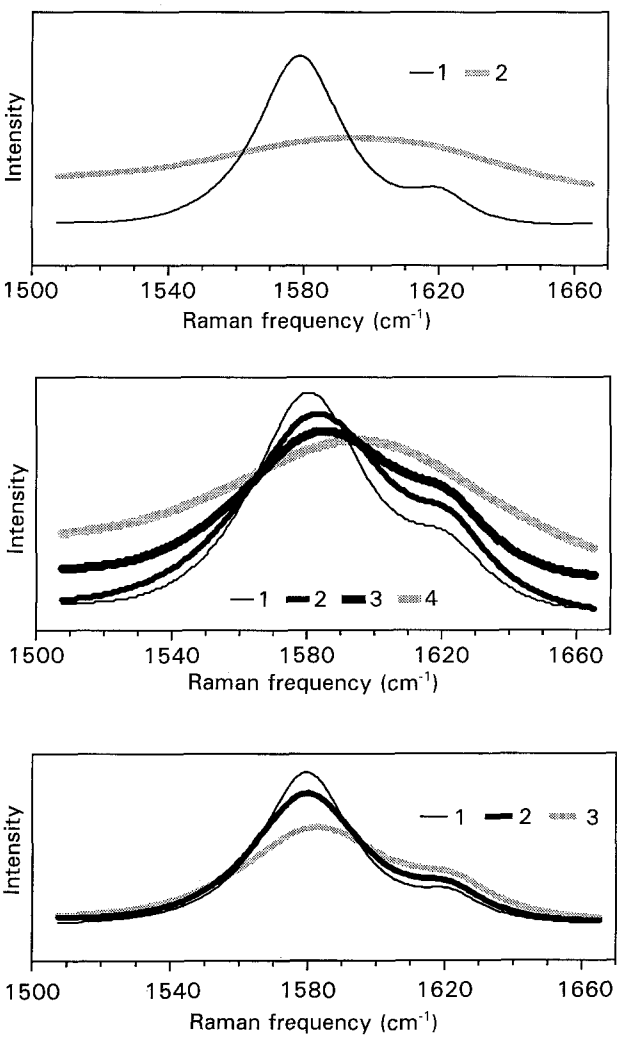

Figure 3 The G-line of the Raman spectrum for (a) the 7 μm in diameter Group A fibres, (b) the 5 μm in diameter Group B fibres and (c) the 5 μm in diameter Group C fibres.

TABLE IV Raman characterization of carbon fibres

Fibre	Group	Raman frequency G-line (cm^{-1})	FWHM (cm^{-1})	Intensity ratio I_D/I_G
1		1580	32	0.35
	A			
2*		1598	125	0.80
1		1582	42	0.60
	B			
2		1584	58	0.85
3		1586	65	0.95
4*		1595	100	0.80
1		1581	35	0.50
	C			
2		1582	42	0.80
3		1584	56	0.95

* In both A2 and B4 fibres the G-line of the spectrum has virtually merged with the shoulder feature D', which explains the shift and broadening of the band.

(c) the higher the fibre modulus and/or crystallinity (Tables I and II), the narrower is the full-width at half-maximum (FWHM) of the G-line of carbon fibres (Table IV).

The A2 and B4 fibres present notable exceptions to the observed trend as both show a dramatic increase in the value of their FWHM and a decrease in their respective l_D/l_G ratios (Table IV). The increase in the FWHM is not surprising because, as mentioned earlier, the G-line in both cases is an unresolved doublet (Fig. 3) and therefore is bound to be broad. Furthermore, the merger of the two lines brings about an apparent increase of the intensity of the G-line which, in turn, causes the l_D/l_G to decrease in spite of the reduction in modulus in both cases (Tables II and III). A detailed Raman spectroscopic analysis of all these fibres will be presented in another publication [33].

4.2. Raman frequency strain dependence in tension and compression

The effect of applied strain upon the G-line of the Raman spectrum of carbon fibres is shown in Fig. 4 for the A1 fibre of Group A. An applied tensile strain of 0.5% causes the G-line to shift by 6 cm^{-1} to lower values of Raman frequency, whereas an applied compressive strain of equal magnitude results in a positive shift of about 5 cm^{-1}. In both cases, the application of external strain brings about a slight broadening of the Raman band which is thought to be due to an increasing stress gradient within the fibre as the applied stress increases [33].

4.2.1. Group A

The Raman frequency shift of the G-line of the A1 fibre, is plotted as a function of applied strain in Fig. 5a. In tension, the Raman frequency decreases with applied strain up to fibre fracture which occurs at about 1.0% strain. At the point of fibre fracture, the local stress is relieved and the Raman frequency increases back to the stress-free value in air (zero frequency shift, Fig. 5a). In compression, the Raman frequency increases with applied strain up to 0.50% strain and, then, it drops back to the stress-free value in air. This frequency drop at 0.55% strain corresponds to a shear-type of fracture as described in detail in the first part of this series [12]. A typical example of such A1 compression fracture is shown in Fig. 6a. At

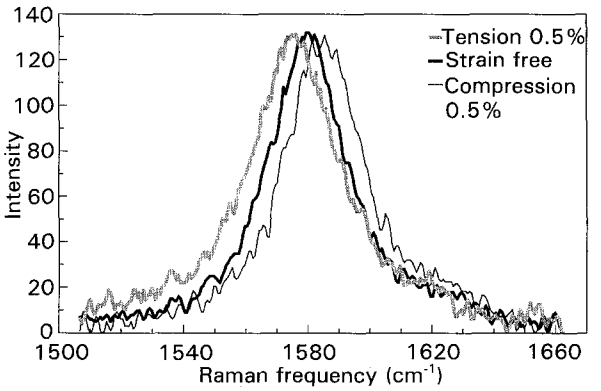

Figure 4 The effect of 0.5% of tensile and compressive on the position of the G-line of the A1 fibre.

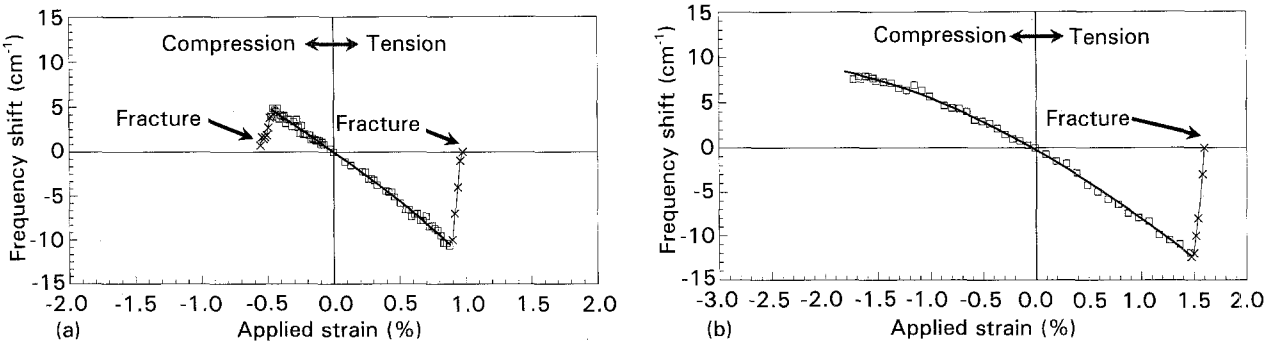

Figure 5 The Raman frequency shift as a function of applied (tensile and compressive) strain for Group A fibres. (a) A1, and (b) A2.

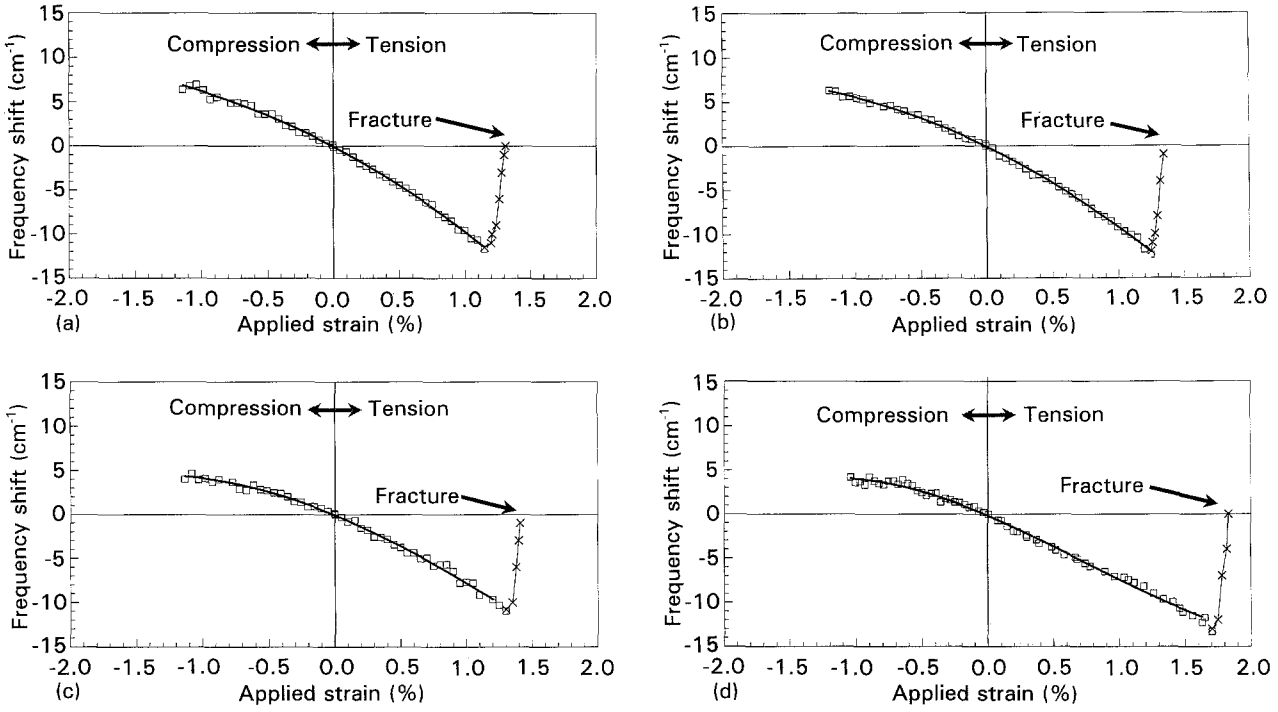

Figure 6 (a) The Raman frequency shift as a function of applied (tensile and compressive) strain for Group B fibres. (a) B1 (b) B2 (c) B3 and (d) B4.

TABLE V Compressive properties of carbon fibres

Fibre	Group	Lower limit of strain for initiation of compressive failure (%)	Predicted upper limit of compressive strain to failure (%)	Lower limit of compressive strength (GPa)	Predicted upper limit of compressive strength (GPa)
1		0.55	–	2.0	–
	A				
2		0.90	2.8	2.0	3.3
1		0.60	2.6	2.2	5.1
	B				
2		0.65	2.0	2.2	3.8
3		0.70	1.3	2.0	2.4
4		0.75	1.2	1.8	2.2
1		0.55	–	1.7	–
	C				
2		0.60	1.2	1.9	2.5
3		0.65	1.4	2.0	2.8

higher applied strains, the maximum strain in the fibre is recovered fully before a new fracture occurs [12]. The values of the critical strain to compressive failure for all the fibres of the group are displayed in Table V.

The behaviour of the A2 fibre differs from that of the A1; the strain sensitivity of the Raman frequency is now notably reduced (Fig. 5b) and no catastrophic failure, manifested by a dramatic drop of Raman

frequency, is observed up to an applied strain as high as 1.6% (Fig. 5b). However, optical microscopic observations during the test have occasionally revealed the formation of tiny "bulges" in the fibre [12]. The lowest ever observed strain for fibre bulging was 0.9% for the A2 fibre. Laser Raman scanning along this region [43] has shown that the Raman frequency drops at the centre of the bulge and recovers sharply at the outer boundaries. Such frequency drops have also been detected during single-fibre cantilever experiments [12] although the incremental step used in scanning the fibre is only rarely coincidental with a bulge. These frequency drops are "lost" in Fig. 5b as these results represent average values from five separate experiments. The important point to note here is that the average Raman frequency still increases with compressive strain regardless of bulge formation.

The Raman frequency shift versus applied strain data of Fig. 5a and b, have been fitted with third degree polynomial regressions. The data points corresponding to either tensile or compressive failure regions, were not included in the regression analysis. The polynomial coefficients and hence the equation of each curve for all the fibres examined in this work, are given in Table VI. An inspection of the values of coefficient of correlation r^2 (Table VI) for all the fibres shows that third degree polynomial functions represent excellent fits to the Raman frequency versus applied strain data.

4.2.2. Group B

The Raman frequency shift is plotted as a function of applied strain for this group of fibres in Fig. 6a–d. None of these fibres failed by shear cracking and bulge formation was present in most cases. The critical strain required for bulge formation (Table V) varies between 0.55% strain for the B1 of tensile modulus of 405 GPa to 0.75% for the B4 of tensile modulus of 305 GPa. It is worth adding here that about 30% of the fibres tested showed no signs of bulging up to the maximum applied strain level to which they were taken (Fig. 7a–d). Furthermore, as in the case of the fibres of Group A which "failed" by bulging, the average Raman frequency increases with compressive strain up to quite high values of strain and third degree polynomial functions can describe well the relationship between Raman frequency and strain in both tension and compression regimes.

4.2.3. Group C

The Raman frequency shift as a function of applied strain for the fibres of this group, is plotted in Fig. 7a–c. The most significant result here is that each of the three fibres exhibits a quite distinct behaviour in compression (Table V) in spite of the similarity of their behaviour in tension (Table II). This clearly shows that the mechanical behaviour of carbon fibres in compression depends largely on their structural characteristics which are, in turn, a consequence of changes in the manufacturing process. In particular, C1 (Fig. 7a) failed predominantly by shear fracture, although some bulges were also observed at high strain levels. By contrast, C3 (Fig. 7b), and C2 (Fig. 7c) fibres did not fail by fracture, but exhibited only localized bulging phenomena. The sensitivity of the Raman frequency shift to applied strain which is expressed by the f_1, f_2 and f_3 coefficients of Table VI, is distinctly different for all the three fibres; in general, the higher the fibre crystallinity (Table IV) the greater is the strain sensitivity of the Raman frequency to applied strain (Table VI).

TABLE VI Polynomial regression of the Raman frequency shift vs applied strain data

Fibre	Degree of polynomial	f_0/ (cm^{-1})	f_1/ ($cm^{-1}/\%$)	f_2/ ($cm^{-1}/\%^2$)	f_3/ ($cm^{-1}/\%^3$)	r^2
A1	2	0.05	− 10.60	− 1.42	−	0.9980
	3	0.02	− 10.45	− 0.93	− 0.86	0.9985
A2	2	− 0.18	− 6.72	− 1.1	−	0.9987
	3	− 0.25	− 6.81	− 1.0	0.06	0.9991
B1	2	− 0.07	− 7.98	− 1.67	−	0.9991
	3	− 0.07	− 7.95	− 1.67	− 0.04	0.9991
B2	2	− 0.08	− 7.41	− 1.74	−	0.9994
	3	− 0.08	− 7.43	− 1.74	0.02	0.9994
B3	2	− 0.11	− 5.97	− 1.72	−	0.9974
	3	− 0.10	− 6.26	− 1.72	0.29	0.9977
B4	2	− 0.13	− 6.3	− 1.83	−	0.9940
	3	− 0.19	− 6.45	− 1.53	0.71	0.9986
C1	2	− 0.40	− 8.73	− 2.0	−	0.9987
	3	− 0.34	− 8.86	− 2.6	0.77	0.9988
C2	2	− 0.02	− 7.35	− 1.98	−	0.9976
	3	− 0.04	− 8.11	− 1.96	0.92	0.9987
C3	2	− 0.17	− 6.15	− 1.56	−	0.9981
	3	− 0.19	− 6.45	− 1.44	0.41	0.9984

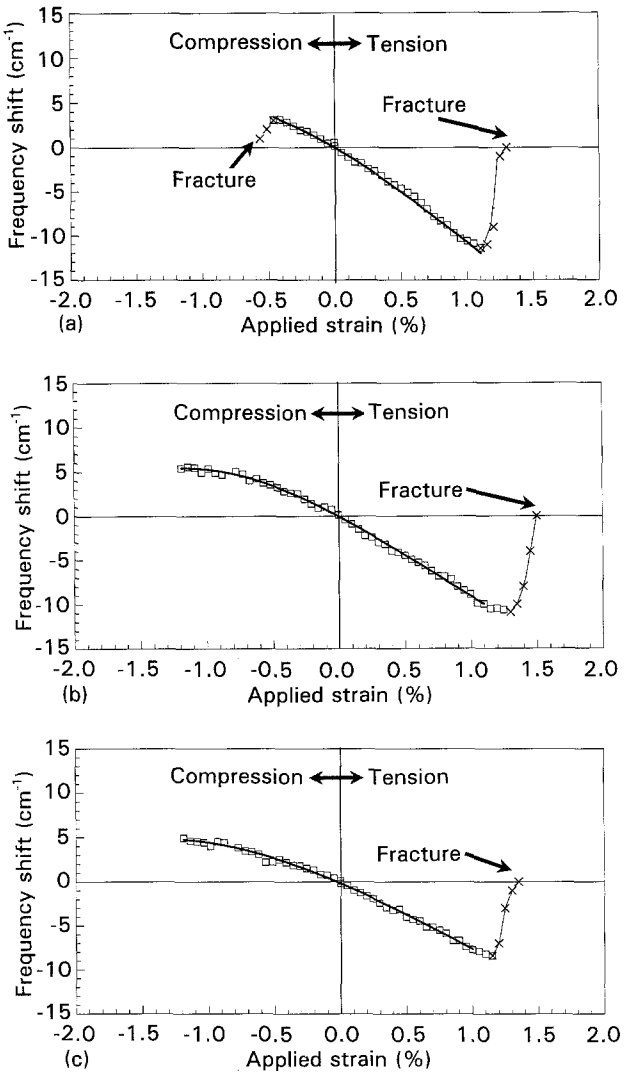

Figure 7 The Raman frequency shift as a function of applied (tensile and compressive) strain for Group C fibres. (a) C1 (b) C2 (c) C3.

5. Discussion

5.1. Raman frequency strain dependence

In the first paper of this series [12], the tension and compression regimes were considered separately and, in each case, the Raman frequency was assumed to be linearly related to the applied strain. As a result of this early approach, a constant value for the compression modulus was derived which was always lower than the initial measured modulus in tension [12]. A more realistic analysis which considers the Raman frequency versus strain relationship to be a smooth and continuous function through the zero-strain point, is attempted here.

As mentioned earlier, the Raman data in tension and compression of Figs 5–7, can be fitted well with third degree polynomial regressions of the form

$$\Delta\nu = f_0 + f_1\varepsilon + f_2\varepsilon^2 + f_3\varepsilon^3 \quad (1)$$

where $\Delta\nu$ is the Raman frequency shift from the value of the stress-free fibre in air and f are the polynomial coefficients which are listed in Table VI. The sensitivity of the Raman frequency to an applied strain, $\alpha_{(\varepsilon)}$, can be represented by the first derivative of the above equation

$$\alpha_{(\varepsilon)} = \frac{d\Delta\nu}{d\varepsilon} = f_1 + 2f_2\varepsilon + 3f_3\varepsilon^2 \quad (2)$$

The shift of the Raman frequency, $\Delta\nu$, for a given fibre/vibrational mode, is only due to the stretching of covalent bonds along the chain and is not affected by rotational or shearing motions. It follows that if the fibre is considered as an aggregate of parallel arrays of identical fibrils consisting of crystallites arranged in series, then for small deformation

$$\Delta\nu = k\sigma \quad (3)$$

where k represents the sensitivity of the Raman frequency shift to an applied stress. Equation 3 clearly states that each group of carbon fibres subjected to identical carbonization drawing conditions but different UFT (Table I), should have one value of k regardless of their respective crystallinity and Young's moduli. By contrast, fibres of Group C which have been subjected to different carbonization drawing regimes should not obey Equation 3.

If Equation 3 is valid, by differentiation we obtain

$$d(\Delta\nu) = k\,d\sigma \quad (4)$$

Furthermore, by dividing both terms by the axial strain differential, $d\varepsilon$, we obtain:

$$\alpha_{(\varepsilon)} = \frac{d(\Delta\nu)}{d\varepsilon} = k\frac{d\sigma}{d\varepsilon} = kE_{(\varepsilon)} \quad (5)$$

where $E_{(\varepsilon)}$ is the strain-dependent axial modulus.

In Fig. 8, the first derivative of the Raman frequency shift with respect to strain for $\varepsilon = 0$, is plotted against the initial Young's modulus for all three groups examined in this work. The connecting line of the two Group A fibres has a slope of $-2.3\,cm^{-1}\,GPa^{-1}$. The data points of Group B fibres which, in addition to thermal treatment, have been subjected to high-level of drawing in the pre-stabilization stage and held at constant length during carbonization and graphitization, can be fitted with a linear regression of slope of $-1.7\,cm^{-1}\,GPa^{-1}$. Finally, the data points for Group C fibres cluster, within experimental error, around the Group B line. It is worth noting, however, that (a) the C1 fibre which has been allowed to shrink during carbonization (Table III), deviates towards the Group A line (Fig. 8), (b) the C2 fibre which has kept at constant length lies closer to Group B line, and finally (c) the C3 fibre which has been subjected to carbonization drawing (Table III), lies above the Group B line (Fig. 8).

The linear relationship between the parameter $\alpha_{(\varepsilon)}$ and the initial modulus, E_0, for at least Group B fibres, confirms the validity of Equation 5 and, hence, Equation 4 for a whole range of tensile moduli. The difference in the value of the slope k (Equation 5, Fig. 8) for

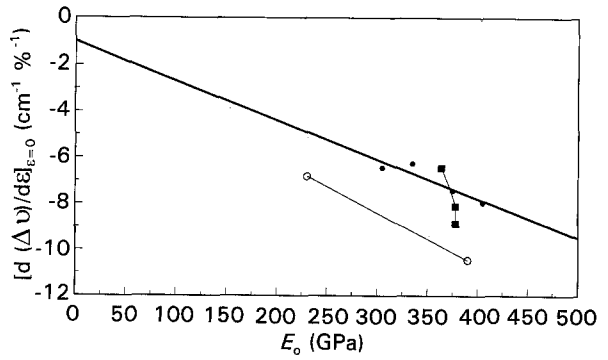

Figure 8 The rate of change of the Raman frequency shift with respect to an applied axial strain as a function of the initial Young's modulus.

the two groups of fibres reflects the significant structural differences arising from the two different carbonization regimes (i.e. shrinkage versus constant length). The latter is further demonstrated in the case of Group C where the data points lie on a "vertical" line (Fig. 8), as the carbonization regime changes from fibre to fibre (Table I). It is also worth mentioning here that the least-squares-fitted lines for both Groups A and B (Fig. 8) do not pass through the origin. This may be indicative of the fact that at the onset of the carbonization regime where the modulus is practically zero, the fibres are kept under tension. In addition, slight discrepancies may arise from the fact that the penetration depth of the Argon laser is only of the order of 50 nm, whereas the initial tensile modulus, E_0, which the Raman data are plotted against, represents an average value across the whole fibre diameter [43].

5.2. Modulus softening in compression and prediction of the critical compressive strain to failure

As stated in Equation 5, the parameter $\alpha_{(\varepsilon)}$ scales with the first derivative of applied stress with respect to strain or, in other words, with the strain-dependent modulus, $E_{(\varepsilon)}$, of the two groups of carbon fibres. Furthermore, the parameter $\alpha_{(\varepsilon)}$, can be defined for any level of fibre strain through the polynomial regressions of Equation 1 of Figs 5–7. Therefore, if E_0 is the initial tensile modulus of the fibres and α_0 is the corresponding value of the first derivative of the Raman data at approximately 0% strain, then from Equation 5, an estimate of modulus $E_{(\varepsilon)}$ at any value of strain (compressive or tensile) can be obtained from the equation

$$E_{(\varepsilon)} = E_0 \frac{\alpha_{(\varepsilon)}}{\alpha_0} \quad (6)$$

In Figs 9–11 the estimated modulus in tension and compression is plotted against the applied strain for the fibres of Groups A, B and C, respectively. In tension, modulus estimates have been obtained up to the strain required to cause brittle fracture. In compression, modulus estimates have been obtained up to the strain required to cause fracture by shear and if fracture is not observed, the value of strain required to obtain "zero" modulus has been determined by extrapolation. The latter represents the upper estimate of compressive strain, ε_{max}, for fibres exhibiting bulging but can still be loaded in compression beyond the limit of 1.3%–1.5% strain imposed by the testing method. Values of ε_{max} for all the fibres tested in this work are listed in Table V.

In general, the results presented in Figs 9–11, show that the modulus of almost all carbon fibres of this work increases with strain in tension while the reverse effect is observed in compression. As it was argued in the first part of this series, if the fibre is regarded as a chain of crystallites each with a slight misorientation with respect to the fibre axis, then the application of a tensile load will tend to align the crystallites in the loading direction, whereas the application of a compressive load will tend to align the crystallites normal to the loading direction. However, as will be shown below, the exact form of the modulus versus strain function can vary from fibre to fibre as it depends upon the fibre precursor and structure, as well as upon the nature and size of imperfections such as voids.

5.2.1. Group A (Fig. 9)

The A1 fibre, which is the fibre with highest surface crystallinity, exhibits strain-hardening effects in tension but only marginal strain softening in compression. Because this fibre is known to possess skin–core morphology [33] the true value of surface modulus at 0% should be higher than 390 GPa. Nevertheless, in spite of the uncertainty regarding the exact values of surface modulus, the A1 modulus versus strain curve of Fig. 9 is considered to be characteristic for all 7 μm high-modulus fibres which fail by shear fracture in compression [36]. By contrast, in the case of the low-crystallinity A2 fibre, the modulus scales linearly with strain. The predicted upper limit of compressive strain to failure of 2.8% for the A2 fibres represents the highest value of strain to failure recorded in this work. In an attempt to provide further experimental evidence for this finding, single A2 filaments have been subjected to over 3% compressive strain on a specially made cantilever beam. The results, which will be presented in the third part of this series [43], confirmed the validity of our predictions and, more import-

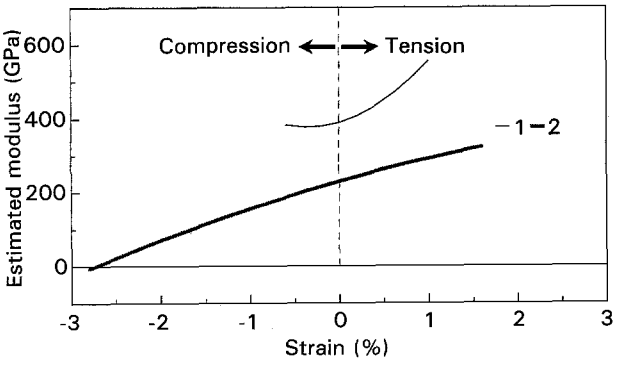

Figure 9 The estimated Young's modulus as a function of applied axial strain for Group A fibres.

antly, provided evidence for the existence of true compression microcracking at 2.8% strain and beyond [43].

5.2.2. Group B (Fig. 10)

The strain dependence of Group B fibres is indeed quite different to the behaviour examined above, in that (a) no fracture by shear is observed, and (b) the higher the fibre initial modulus the higher is the upper of limit of compressive strain to failure. Again it is interesting to note that the low-modulus B4 fibre exhibits only a moderate strain-hardening effect in tension up to approximately 0.8% strain, followed by a modulus drop to its original value (Fig. 10). Regarding softening in compression, both B4 and B3 fibres exhibit a quite dramatic reduction in modulus, resulting in relatively low values of maximum compressive strain to failure of 1.2% and 1.3% (Table V), respectively. However, what is indeed remarkable here is the fact that the high-modulus fibres of this group, namely B2 and B1, exhibit a significantly lower rate of modulus softening in compression and hence high values of maximum compressive strain to failure (Table V).

5.2.3. Group C (Fig. 11)

The C1 fibre, which has been heat-treated at high firing temperatures, fails by shear fracture in compression and exhibits the same rate of modulus hardening and softening in tension and compression, respectively. By contrast, the C2 and C3 fibres which have been treated at lower firing temperatures, soften at lower rates in compression and exhibit only bulging formations at low applied strains. The results for this group of fibres which have almost identical initial moduli but different structures, show quite clearly that by applying low firing temperatures and by controlling the morphology of the precursor, one can achieve (a) a change of mode of failure in compression, (b) a reduction to the rate of modulus softening in compression, and (c) higher values of maximum compressive strain to failure.

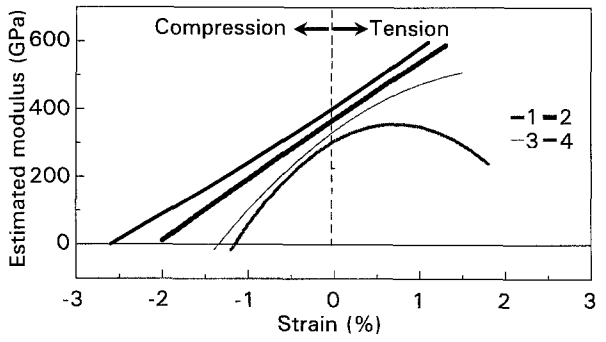

Figure 10 The estimated Young's modulus as a function of applied axial strain for Group B fibres.

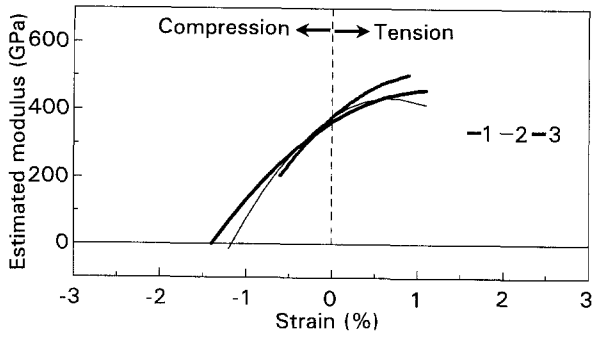

Figure 11 The estimated Young's modulus as a function of applied axial strain for Group C fibres.

5.3. Fibre stress–strain curves in tension and compression

Because an estimate of the modulus can be produced at any strain level then a stress–strain function can also be derived by integration

$$\sigma_{(\varepsilon)} = \int F_{(\varepsilon)} d\varepsilon \quad (7)$$

or, finally, by substituting Equation 6 into 7

$$\sigma_{(\varepsilon)} = \int E_0 \frac{\alpha_{(\varepsilon)}}{\alpha_0} d\varepsilon$$

$$= \frac{E_0}{\alpha_0} \int \alpha_{(\varepsilon)} d\varepsilon \quad (8)$$

Equation 8 has a general validity and can be used to convert any Raman frequency versus strain data into stress versus strain data, regardless of the form of the $\alpha_{(\varepsilon)}$ function. In Figs 12–14, the predicted stress–strain curves for Groups A, B and C are shown and the corresponding predicted upper limits of compressive stress/strain to failure, are given in Table V.

The results for Group A (Fig. 12) show that the higher the ultimate graphitization temperature (UFT), the greater the amount of pivoting of the stress–strain curve around the origin and hence the higher the modulus in both tension and compression regimes. Furthermore, an increase of graphitization temperature to 2600 °C for the A1 fibre leads to catastrophic fracture in shear at relatively low values of compressive stress. By contrast, the A2 fibre which has been heat treated at lower temperatures can be potentially loaded to quite high values of stress and strain in compression (Table V). In fact, as mentioned earlier, the predicted upper limit of compressive strength of

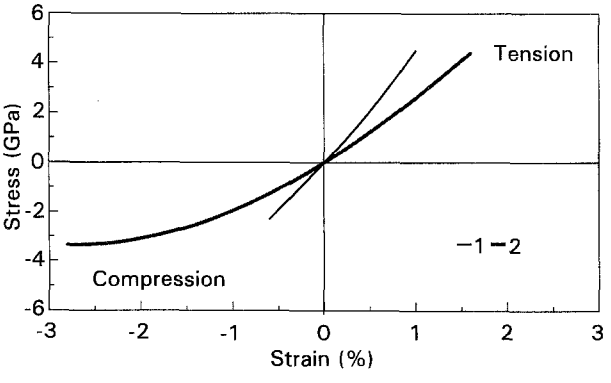

Figure 12 The predicted stress-strain curves for Group A fibres.

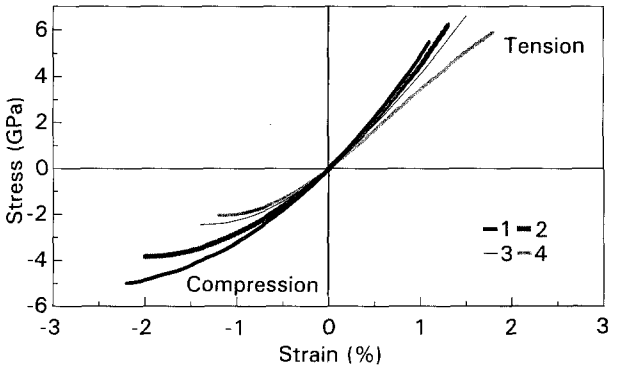

Figure 13 The predicted stress-strain curves for Group B fibres.

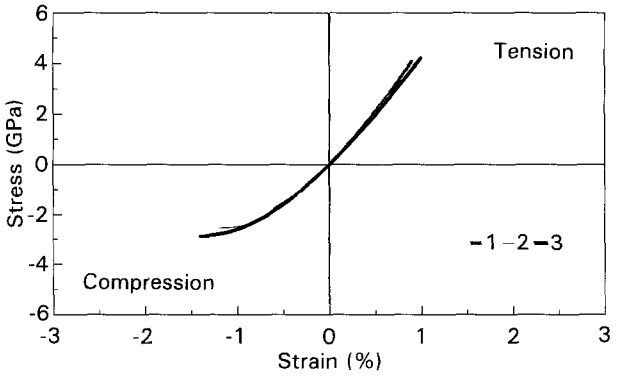

Figure 14 The predicted stress-strain curves for Group C fibres.

3.3 GPa obtained for the A2 fibre, has been verified by loading the A2 fibre to 3% compressive strain on a specially made cantilever beam [43].

The results for Group B presented in Fig. 13, are indeed striking. The stress–strain curves pivot around the origin as in the case of Group A fibres but it seems that high-modulus fibres like B2 and B1 can survive very high values of compressive stress/strain which can be as high as their predicted strength in tension. On the contrary, the fibres produced at lower graphitization temperatures such as B4 and B3, exhibit an upper limit of compressive strength which is not very much higher than 2 GPa. In other words, as very high graphitization temperatures promote fracture by shear to fibres of Group A, very low graphitization temperatures promote fibre "yield" or "collapse" at relatively low values of stress/strain to fibres of Group B.

Finally, the upper compressive stress/strain to failure for the fibres of Group C increases as the amount of hot-stretching increases (Fig. 14) and therefore lower graphitization temperatures (Table III) are employed to achieve the same value of modulus at zero strain.

5.4. Fibre morphology and mode of failure in compression

Over the last few years there have been many attempts to relate carbon fibre compressive strength to various structural parameters such as crystallite thickness and aspect ratio [44–46]. More recently some evidence has emerged relating the compressive strength of all

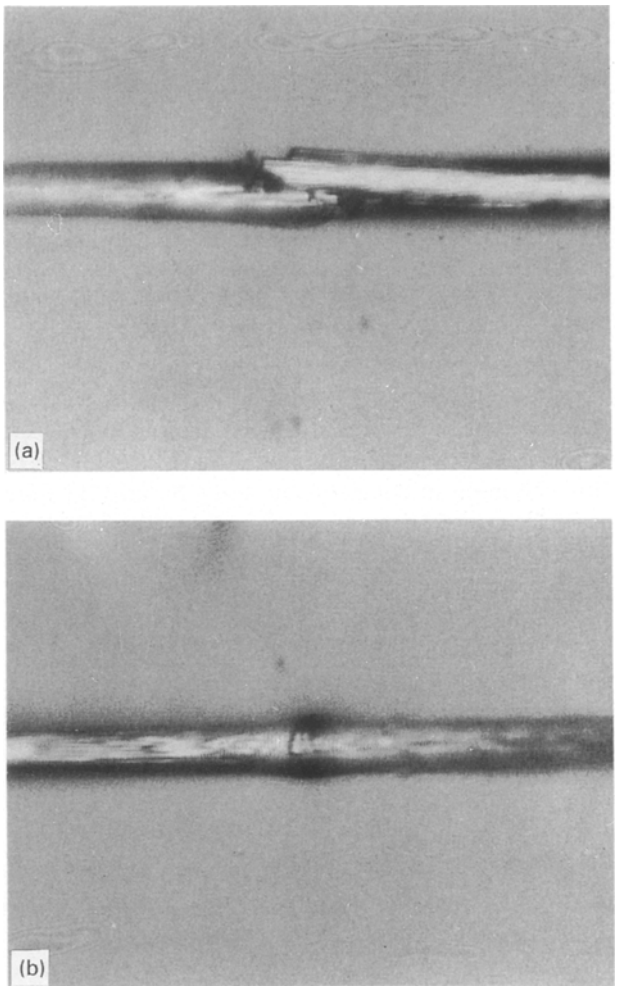

Figure 15 (a) Sketch of the shear-like fracture of the highly crystalline A1 fibre in compression. The fibre diameter is 7 μm. (b) Sketch of fibre 'bulging' in compression for an A2 fibre. The fibre diameter is 7 μm.

carbon fibres to crystal cross-sectional area per unit length [47]. Similarly, the results presented here show quite clearly that the combination of precursor drawing and thermal treatment, has a profound effect upon the structure of the fibres which, in turn, triggers a particular type of compression failure. In particular, high graphitization temperatures encourage the growth of large crystals and induce skin–core heterogeneity [36]. The fibres of this category such as the A1, fail in shear at an angle of about 45° to the fibre axis (Fig. 15a). This mode of failure normally occurs at low compressive strains to failure and is associated with the intrinsic sheet-like or ribbon-like structure of these fibres. It seems that these highly oriented layers of graphite are vulnerable to Eulerian (buckling) instabilities, in accordance with earlier observation [16, 17]. On the other hand, low graphitization temperatures combined with further thermal drawing, lead to smaller crystals (Table III) and much less pronounced skin–core effects. The fibres of this category contain crystallites of low aspect ratio or cross-sectional area per unit length [47] and, therefore, can survive much higher compressive loads. As mentioned earlier, the bulging formation at relatively low strains is a form of local failure and it does not affect the load-carrying capability of the fibre. Recent model work has shown

[43] that this form of failure is encouraged by the absence of lateral support during cantilever loading of single filaments and, therefore, should not be present in fibres embedded in full composites. However, the very appearance of bulging in fibres compressed in air or under a thin layer of acrylic film (Section 3.2), indicates that these fibres respond to the application of axial loading by crystallite rotation and shearing and this is also evident in the linear reduction of modulus with applied strain (Fig. 10). Finally, the much lower graphitization temperatures employed to produce B3 and B4 fibres, yield crystallites which rotate in an unstable fashion under the influence of an applied stress and this results in a sharp drop in compression modulus and fibre collapse, at relatively low values of strain (Fig. 10).

The results presented in this paper, show unequivocally that for the attainment of high compressive stresses to failure, there is an optimum window of graphitization temperatures specific to each fibre precursor which has to be employed. In general, low graphitization temperatures and control of modulus by precursor drawing, can yield fibres with a truly exceptional compressional performance. This is clearly shown in Fig. 16 where the estimated compressive strength is plotted as a function of the initial tensile modulus for all the fibres examined here. As is evident, no apparent trend between estimated compressive strength and initial modulus, is observed. However, a careful examination of the results show that whereas for Group A fibres the estimated compressive strength generally decreases with modulus, for Group B fibres the reverse trend is obtained. Thus, the optimum window of graphitization temperatures for the precursor of Group A is that employed for the A2 fibres and for the precursor of Group B, that employed for the B1 fibres at a much higher modulus value. Similarly, by increasing thermal drawing while decreasing the graphitization temperature, an improvement of the compressive strength for the same initial modulus can be obtained as in the case of Group C fibres.

As mentioned earlier, laser Raman spectroscopy is an ideal tool not only for assessing the mechanical behaviour of carbon fibres but also for structural characterization of their surfaces. Because the initial tensile modulus of a carbon fibre is not necessarily indicative of its mode of failure in compression (Fig. 16), an attempt has been made to relate the mode of failure in compression to the ratio of the intensities R ($\sim I_D/I_G$) which, as mentioned earlier, is related to (a) crystallite size, and (b) crystallite orientation, at the carbon fibre surface.

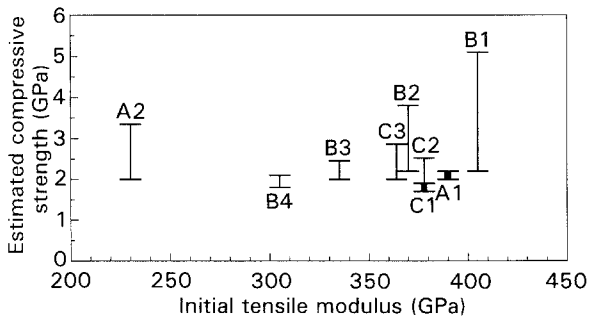

Figure 16 The estimated compressive strength as a function of the initial tensile modulus.

In Fig. 17, the sensitivity of Raman frequency of the G-line is plotted as a function of the intensity ratio, R. As can be seen, the Raman frequency strain dependence in absolute numbers, is approximately inversely proportional to the intensity ratio. This again demonstrates that the higher the surface crystallinity the greater the amount of bond stretching resulting from an applied axial strain and vice versa, i.e. the lower the surface crystallinity the greater is the crystallite rotational and shearing motions and, hence, the lesser is the amount of bond stretching. It is interesting to note that for $R > 0.5$ the fibres exhibit bulging whereas for $R < 0.5$ catastrophic failure in terms of fracture in shear occurs. The C1 which has $R = 0.5$ exhibits both bulging and shear fracture and therefore is considered to be at the threshold of the transition between the two types of compressional behaviour examined here.

5.5. The effect of fibre compression modulus softening on full composites

As mentioned in the early sections of this paper, observations of strain softening in compression, in unidirectional carbon fibre/epoxy composites have been ascribed to the strain softening of the fibres themselves [2–4]. Having produced an estimate for the fibre compressive modulus and the fibre stress at any level of compressive strain, it was thought essential to compare these findings with those obtained from full composite testing.

In a recent paper by Haeberle and Matthews [4], the tangent longitudinal compressive modulus of a unidirectional Courtaulds Grafil XAS (A2) carbon fibre/epoxy resin composite 60% in volume fraction, was reported to decrease from an initial value of 129.6 GPa to 55.6 GPa at 1.96% compressive strain, as shown in Fig. 18. The measured stress at that level of compressive strain was 1.93 GPa (Fig. 18). At higher levels of applied load failure was reported to

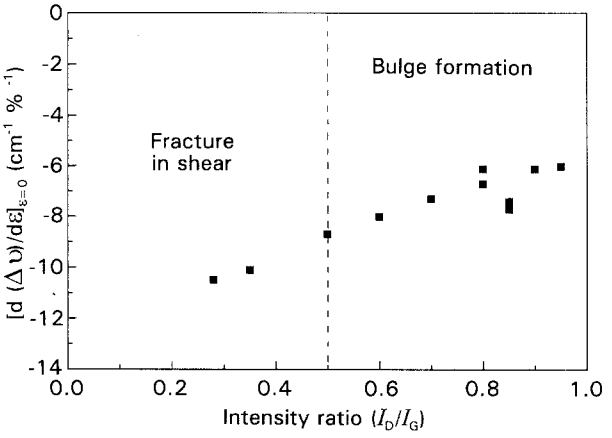

Figure 17 The rate of change of the Raman frequency shift with respect to an applied axial strain as a function of the Raman intensities ratio I_D/I_G. The value obtained from an untreated fibre high modulus fibre (HMU) [36], has also been added.

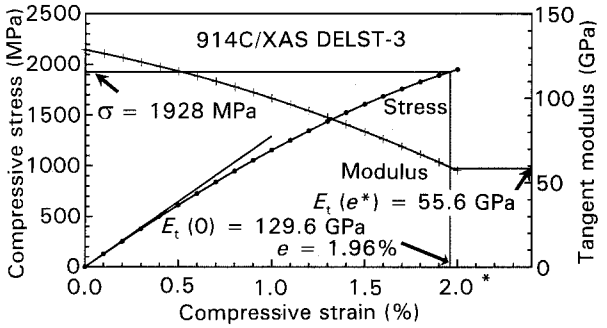

Figure 18 The composite stress and tangential modulus as a function of compressive strain, for a 60% fibre volume fraction XAS (A2) carbon fibre/epoxy resin unidirectional composite (from [4]).

initiate near the grips [4]. By employing the rule of mixtures

$$E_{\text{composite}} = E_{\text{fibre}} V_{\text{fibre}} + E_{\text{matrix}}(1 - V_{\text{fibre}}) \quad (9)$$

a fibre modulus of 90 GPa was deduced at 1.96% compressive strain. Similarly, the application of the law of mixtures for the composite stress

$$\sigma_{\text{composite}} = \sigma_{\text{fibre}} V_{\text{fibre}} + E_{\text{matrix}} e_{\text{composite}}(1 - V_{\text{fibre}}) \quad (10)$$

yields a value of 3.2 GPa for the fibre stress at 1.96%. The values obtained in this work, were 3.0 and 74 GPa for the compressive stress and modulus, respectively. Both values are exceptionally close to those deduced from [4] and come to verify the claim that the modulus softening phenomena in compression of carbon fibre/epoxy resin unidirectional composites, are predominantly due to the softening of the fibres themselves.

6. Conclusions

Laser Raman spectroscopic studies on a series of PAN-based carbon fibres, have shown that the axial fibre modulus increases with strain in tension while the reverse effect is observed in compression. Furthermore, it has been demonstrated that for the attainment of high compressive stresses to failure, there is an optimum window of graphitization temperatures specific to each fibre precursor which has to be employed. In general, low graphitization temperatures and control of modulus by precursor drawing, can yield carbon fibres with a truly exceptional compressional performance.

Acknowledgements

This programme of research was funded by grants from the Defence Research Agency (DRA–RAE), the Department of Trade and Industry, Courtaulds Grafil plc, the Science and Engineering Research Council and Queen Mary and Westfield College. The authors thank Dr M. Pitkethly (DRA–RAE), R. R. Robinson (Courtaulds plc) and Dr C. K. L. Davies (QMW) for their useful suggestions and recommendations. Mr F. L. Matthews and Dr J. Haeberle, Imperial College, are thanked for stimulating discussions and for permission to publish the data shown in Fig. 18.

References

1. ASTM D3410-87, "Standard Test Method for Compressive Properties of Unidirectional and Cross-Ply Fiber-Resin Composites", Annual Book of ASTM Standards, Philadelphia, (1989) p. 1996.
2. J. M. WHITNEY, I. M. DANIEL and .R. B. PIPES, "Experimental Mechanics of Fiber Reinforced Composite Materials", The Soc. for Exp. Mechanics, New Jersey (1984).
3. A. S. CRASTO, R. Y. KIM, J. M. WHITNEY, "Composites Testing & Characterisation", ECCM-CTS, eds P. J. Hogg, G. D. Sims, F. L. Matthews, A. R. Bunsell and A. Massiah (ECCM-CTS, Amersterdam, 1992) p. 113.
4. J. G. HAEBERLE, F. L. MATTHEWS (1990), Proc. ECCM'90, Developments in the Science and Technology of Composite Materials, Stuttgart (Elsevier, London, 1990) p. 517.
5. T. B. STECENKO, M. M. STEVANIVIC, *J. Mat. Sci.* **24** (1990) 1152.
6. J. G. HAEBERLE, F. L. MATTHEWS, in the Proceedings of Applied Solid Mechanics-3, April 1989, Guildford (Elsevier Applied Science, London, 1989).
7. G. J. CURTIS, J. M. MILNE, W. N. REYNOLDS, *Nature* **220** (1968) 1024.
8. M. MARTINEZ, M. R. PIGGOTT, D. M. R. BAINBRIDGE, B. HARRIS, *J. Mat. Sci.* **16** (1981) 2831.
9. S. B. BATDORF, in the Proceedings of the International Conference on Composite Materials and Structures, Beijing, China 1986, Ed. T. T. Loo, pp. 746–750.
10. J. D. H. HUGHES, *Carbon* **24** (1986) 551.
11. P. ARSENOVIC, H. JIANG, R. K. EBY, W. W. ADAMS, J. M. LIU, in the Proceedings of CARBON' 88, Ed. McEnaney, T. J. Mays, p. 485 (1988).
12. N. MELANITIS, C. GALIOTIS, *J. Mat. Sci.* **25** (1990) 5081.
13. A. CRASTO, R. KIM and J. WHITNEY, *Int. SAMPE Symposium* **36** (1991) 1649.
14. C. VLATTAS, C. GALIOTIS, *Polymer* **32** (1991) 1789.
15. D. SINCLAIR, *J. App. Phy.* **21** (1968) 380.
16. W. R. JONES, W. J. JOHNSON, *Carbon* **9** (1971) 645.
17. H. M. HAWTHORNE, E. TEGHTSOONIAN, *J. Mat. Sci.* **10** (1975) 41.
18. D. J. BOLL, R. M. JENSEN, L. CORDNER, W. D. BASCOM, *J. Comp. Mat.* **24** (1990) 208.
19. S. J. DeTERESA, R. S. POTTER, R. J. FARRIS, *J. Mater. Sci.* **10** (1985) 1624.
20. S. J. DeTERESA, R. S. POTTER, R. J. FARRIS, *J. Mat. Sci.* **23** (1988) 1886.
21. T. OSHAWA, M. MIWA, M. KAWADE, E. THUSHIMA, *J. App. Pol. Sci.* **39** (1990) 1733.
22. M. G. DOBB, D. J. JOHNSON, C. R. PARK, *J. Mater. Sci.* **25** (1990) 829.
23. J. B. DONNET, R. P. BANSAL, "Carbon Fibres" (Marcel Dekker Inc., New York 1984).
24. M. S. DRESSELHAUS, G. DRESSELHAUS, K. SUGIHARA, I. L. SPAIN, H. A. GOLDBER, "Graphite Fibres and Filaments" (Springer-Verlag, Berlin, 1988).
25. S. C. BENNET, D. J. JOHNSON, Proceedings of London Carbon and Graphite Conference (1978) **1** p. 377.
26. M. GUIGON, A. OBERLIN, G. DESARMOT, *Fibre Sci. and Tech.* **20** (1987) 177.
27. W. RULAND, *J. Appl. Phy.* **38** (1967) 3585.
28. F. TUINSTRA, J. KOENIG, *J. Chem. Phys.* **53** (1970) 1126.
29. F. TUINSTRA, J. KOENIG, *J. Comp. Mat.* **4** (1970) 492.
30. G. KATAGIRI, H. ISHIDA, A. ISHITANI, *Carbon* **26** (1988) 565.
31. P. LESPADE, A. MARCHAND, M. COUZI, F. CRUEGE, *Carbon* **22** (1984) 375.
32. R. P. VIDANO, D. B. FISCHBACH, L. J. WILLIS, T. M. LOEHR, *Solid State Communications* **39** (1981) 341.
33. N. MELANITIS, C. GALIOTIS, submitted to *Carbon*.
34. I. M. ROBINSON, M. JAHIKHANI, R. J. DAY, R. J. YOUNG, C. GALIOTIS, *J. Mat. Sci. Letters* **6** (1987) 1212.

35. C. GALIOTIS, D. N. BATCHELDER, *J. Mat. Sci. Lett.* **7** (1988) 545.
36. N. MELANITIS, PhD Thesis, University of London 1991.
37. R. S. BRETZLAFF, R. P. WOOL, *Macromolecules* **16** (1983) 1907.
38. K. TASHIRO, G. WU, M. KOBAYASHI, *J. Pol. Sci. B*, **28** (1990) 2527.
39. C. GALIOTIS, *Comp. Sci. and Tech.* **42** (1991) 125.
40. UK Patent Application, GB 2084975 Pepper, R. T., Nelson, D. C. and Lewing, D. S. 1981.
41. M. K. JAIN, M. BALASUBRAMANIAN, P. DESAI and A. S. ABHIRAMAN, *J. Mater. Sci.* **22** (1987) 301.
42. S. P. TIMOSHENKO, J. M. GERE, "Theory of Elasticity" (McGraw-Hill, N.Y. 1961).
43. P. L. T. TETLOW, N. MELANITIS, C. GALIOTIS, submitted to *Carbon*.
44. A. S. CRASTO, D. P. ANDERSON, Proc. ASC'90, American Society of Composites (1990) p. 809.
45. S. KUMAR, W. W. ADAMS and T. E. HELMINIAK, *J. Reinforced Plastics* **7** (1988) 108
46. S. KUMAR and T. E. HELMINIAK, "The Materials Science and Engineering of Rigid Rod Polymers", eds Adams W. W., Eby R. K. and McLemore D. E., Mater. Res. Soc. Symp. Proceedings 134 (M.R.S., Pittsburg PA, 1989) p. 363.
47. S. KUMAR, V. R. MEHTA, D. P. ANDERSON and A. S. CRASTO, 37th Int. SAMPE Symp. (SAMPE, 1992) p. 67.

Received 9 February 1993
and accepted 30 May 1993